Near-Infrared Refractive Index of Thick, Laterally Oxidized AlGaAs Cladding Layers

F. Sfigakis, P. Paddon, V. Pacradouni, M. Adamcyk, C. Nicoll, A. R. Cowan, T. Tiedje, and Jeff F. Young

***Abstract*—The optical transmission in the range 900–1600 nm was measured through thick (~1 μm) layers of $Al_{0.98}Ga_{0.02}As$ wet-oxidized at 375 °C on GaAs. The spectra are fit well by neglecting absorption, and using 1.61 for the refractive index.**

***Index Terms*—Oxide-cladding, photonic crystals, refractive index, semiconductor waveguides, wet-oxidation.**

I. Introduction

THE LATERAL oxidation of epitaxially grown layers of Al-rich $Al_xGa_{1-x}As$ is already an important process used in fabricating vertical-cavity surface emitting lasers (VCSEL's), index-guided, in-plane lasers, distributed Bragg reflectors (DBR's), asymmetric Fabry–Perot (ASFP's) modulators, resonant cavity photodetectors, and resonant-cavity light-emitting diodes (RCLED's) [1]–[4]. Many studies on the kinetics of the oxidation reaction and microstructure of the oxide have been published [5]–[10]. However, the vast majority of previous work has concentrated on relatively thin (<100 nm) layers, and there is little information about the optical properties of these oxides in the 0.9–1.55-μm wavelength range. The index of refraction of oxidized AlGaAs or AlAs has been reported [11]–[16], but most of this information is based on single-wavelength ellipsometry (often done at a wavelength of 633 nm).

Thicker layers of oxidized AlGaAs are of interest as low-index cladding layers in waveguide-based "photonic crystals" [17], [18]. It is important to know the complex refractive index of the oxides over a wide (>100 nm) spectral range, corresponding at least to the size of the optical gaps that are opened up in these photonic crystals through the use of periodic dielectric texture [17], [18]. In this paper we describe the successful lateral oxidation of an ~1 μm thick layer of $Al_{0.98}Ga_{0.02}As$ that remains robustly attached to a GaAs substrate. The normalized transmission spectra of broad-band radiation through the oxidized cap layer and the substrate are fit to obtain an estimate of the complex refractive index of the oxide layer in the range 900–1600 nm. The spectra can be fit using a refractive index of 1.61 and zero absorption.

Manuscript received June 29, 1999; revised October 20, 1999. This work was supported by the National Science and Engineering Research Council and the Canadian Cable Laboratories Fund.

The authors are with the Department of Physics and Astronomy, University of British Columbia, Vancouver, BC V6T 1Z1, Canada.

Publisher Item Identifier S 0733-8724(00)01317-7.

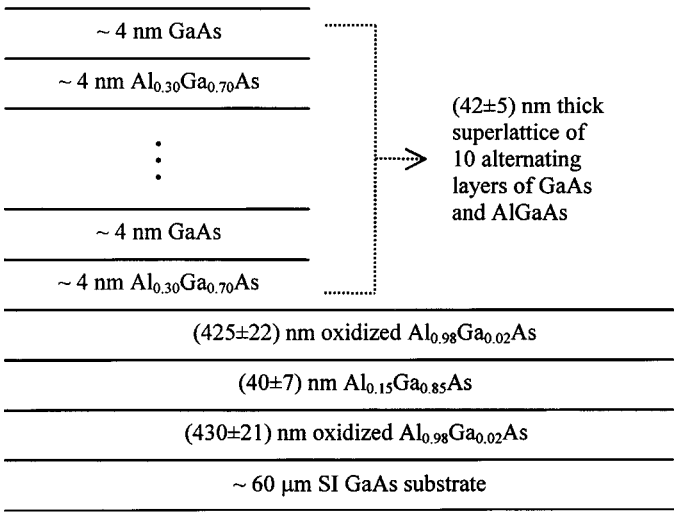

Fig. 1. Structure of the MBE-grown sample.

II. Oxidation Process

The sample used in this study was a passive waveguide structure, grown by molecular beam epitaxy (MBE): its structure is shown in Fig. 1. The semi-insulating GaAs substrate was ground and polished to a total thickness of 60 μm. The epitaxial layer thicknesses shown in Fig. 1 were measured with a scanning electron microscope (SEM), after oxidation. Two layers of oxidized $Al_{0.98}Ga_{0.02}As$, one 430-nm -thick and the other 425-nm thick, surround a 40-nm thick $Al_{0.15}Ga_{0.85}As$ core layer. A superlattice cap made up of ten alternating layers of ~4 nm GaAs and ~4 nm $Al_{0.30}Ga_{0.70}As$ (total cap layer thickness of 42 nm) protected the top cladding layer from exposure to the ambient atmosphere. The nominal aluminum composition of the $Al_{0.98}Ga_{0.02}As$ layers was confirmed by X-ray diffraction (XRD), prior to oxidation. Ridges, ~30 μm wide, were defined by selective wet etching in alternating steps with solutions of $HF:H_2O_3:5000$ and $C_6H_8O_7:H_2O_2$ 50 : 1 (volume ratios); the $C_6H_8O_7$ (citric acid) solution was prepared by mixing $C_6H_8O_7:H_2O$ 1 : 1 by mass. The total etch depth was about 5 μm. Since the epitaxial layers are ~1-μm thick, this means that the etched troughs extended approximately 4 μm into the substrate. The oxidation process was carried out for 90 min in a N_2/H_2O atmosphere at a temperature of 375 °C. The oxidation reaction propagated laterally in the oxidized layer via the exposed edges of the ridges.

SEM and AFM measurements show that the oxidized $Al_{0.98}Ga_{0.02}As$ layers contract by (5.4 ±0.9)%. Energy-dispersive X-ray spectroscopy indicated that the oxide layers are

composed of aluminum oxide with a small amount of residual gallium. Powder X-ray diffraction measurements show no sign of crystalline structure. Based on these data and similar published results [5]–[8], we hypothesize that our oxide films are predominantly made up of amorphous aluminum oxide, possibly hydrogenated, and possibly containing small, <10 nm, Al_2O_3 crystals.

The lateral oxidation of our thick $Al_{0.98}Ga_{0.02}As$ layers followed a linear growth law for temperatures between 375 °C–450 °C, characteristic of a reaction rate-limited process. This is consistent with the observations of others [10]. The simplest function that phenomenologically describes the oxidation rate is

$$\kappa(T, \delta) = \kappa_o(\delta) \cdot \exp\left[\frac{-E_a(\delta)}{k_B T}\right] \tag{1}$$

- κ linear oxidation rate;
- κ_o prefactor;
- k_B Boltzmann constant;
- E_a activation energy of the reaction mechanism;
- δ thickness of the unoxidized layer.

By fitting the rate constants measured over this range of temperatures to (1), we obtain an activation energy of $E_a = (1.56 \pm 0.03)$ eV and a value of 2.9 $\pm$1.3 $\times$ 10^{13} μm/h (8 $\pm$ 3 $\times$ 10^3 m/s) for κ_o. These results are consistent with those reported by others, using thinner AlAs layers [9], [10]. Fig. 2 shows the values obtained in the present work, together with those reported by other groups, as a function of the AlAs layer thickness.

Although it is possible to oxidize the samples at temperatures as high as 450 °C, delamination becomes more of a problem than at lower temperatures. The lack of run-to-run reproducibility in regard to delamination, also reported by Evans *et al.* [19], makes it difficult to identify precise conditions under which it can be reliably avoided. However, our experience indicates that the key is to oxidize completely through the ridge in a single high-temperature process, but to stop as soon as possible after the oxidation fronts meet at the center of the ridge. If the oxidation rate is not well characterized, it is difficult to avoid "over-oxidizing" at higher temperatures, and hence we find that lower temperatures usually produce more reliable results. SEM studies of partially oxidized mesas may indicate why it is important to completely oxidize the ridges in a single process step, as also noted by Evans *et al.* [19]. We find that cross-sections of partially oxidized ridges routinely show good quality interfaces behind the oxidation fronts, but there is always some degree of local delamination near the fronts. When two oxidation fronts collide at elevated temperatures it seems that the single resulting oxide layer can conform to the unoxidized substrate, whereas incomplete penetration leaves two locally delaminated fronts that can nucleate more massive delamination if cooled too rapidly, or if subject to further thermal processing.

III. Optical Transmission Measurements

A halogen lamp filament was imaged into a single mode optical fiber, and the output of the fiber was weakly focused on the processed wafer surface, at normal incidence. A magnified image of the ridges, obtained through the substrate, was projected onto the entrance aperture of a BOMEM DA8 Fourier

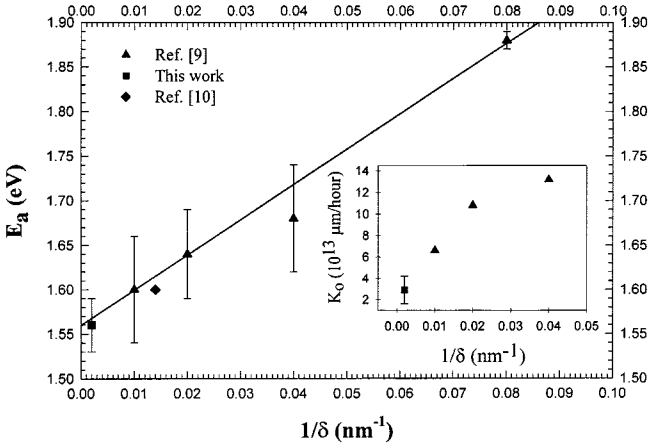

Fig. 2. Activation energies as a function of thickness from various research institutions; the inset shows the prefactor as a function of layer thickness.

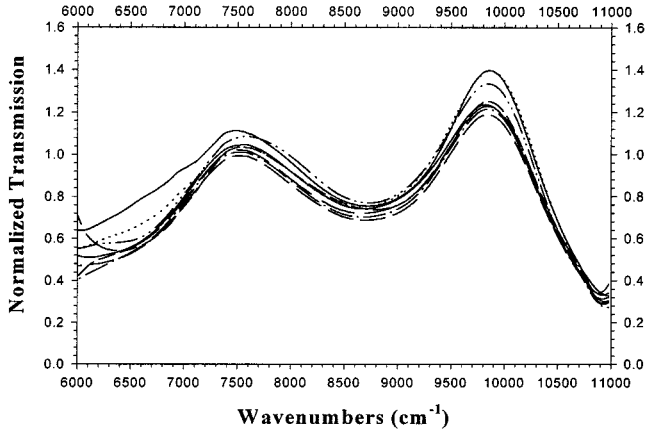

Fig. 3. Eight normalized, normal incidence transmission spectra. As discussed in the text, the normalization consists of dividing the spectrum through a ridge by the spectrum through the substrate.

transform interferometer. By adjusting the size and location of the input aperture, it was possible to separately measure the transmission spectrum of the light passing through the substrate and the oxidized layers in the ridges, or through the substrate alone. The spectra were obtained at a low resolution of 40 cm^{-1}, which served to remove the modulation due to Fabry–Perot effects in the substrate. The transmission spectra obtained through the ridges were then normalized by spectra taken through the adjacent substrate. This was a convenient normalization procedure since the transmission spectrum through a single slab of semi-insulating GaAs is easily modeled. All normalized transmission spectra were generated in pairs: the first one would be through a ridge, followed immediately by a scan through the substrate between the ridges, without adjusting any of the optics.

Fig. 3 shows eight normalized transmission spectra taken over a period of several hours from different locations on more than one ridge. Because none of the optical elements were adjusted between the reference scan through the substrate and the scan through the ridge, both the spectral positions of the features in the transmission spectra, and their amplitudes could be used to estimate the complex refractive index of the oxide layers. The dashed lines in Fig. 4 show the $\pm 3\sigma$ uncertainty range about

the *average* of the eight spectra shown in Fig. 3, where σ is the frequency-dependent standard error in the data.

IV. Refractive Index Determination

The normalized transmission spectra were simulated using a simple multilayer solution of the Maxwell equations at normal incidence. Two simulations were done for each spectrum, one for the reference transmission through the uniform slab of semi-insulating GaAs, and the other for the actual ridge data. The simulated spectra were filtered (in position space) to simulate the 40 cm^{-1} resolution of the interferometer. The known dispersion of the refractive indexes of GaAs and $Al_{0.15}Ga_{0.85}As$ layers were included [20]. The thicknesses of the layers were determined by SEM measurements, but the fitting procedure allowed their values to vary within the uncertainty shown in Fig. 1. Thus, allowing for the uncertainties in the layer thickness, the only remaining "free" parameter is the aluminum oxide's refractive index.

Fig. 4 shows the simulated spectrum that is closest to falling within the $\pm 3\sigma$ uncertainty range of the experimental data shown in Fig. 3.

This fit was obtained by neglecting dispersion in the oxide's refractive index, so no attempt was made to include it (note that the refractive index of α-alumina varies only from 1.755 to 1.746 between 1033–1550 nm [21]). The best fits were generated with indexes of refraction varying from 1.59 to 1.63 for the oxidized $Al_{0.98}Ga_{0.02}As$ layers. Both layers have the same index of refraction; this was not enforced, but came naturally out of the fitting process. Even though the SEM images indicated that the thicknesses of both $Al_{0.98}Ga_{0.02}As$ layers were similar (within 5 nm), the fits were optimum with asymmetric thicknesses (consistent with SEM uncertainties). For each different value of the oxide's index of refraction in the range 1.59–1.63, the difference between the thicknesses of the oxide layers remained consistently in the ~40 nm range. Table I gives the parameters associated with the best fits obtained using indexes of refraction of 1.59, 1.61, and 1.63, along with the thicknesses measured using the SEM.

Fig. 5 shows a plot of the sum-of-squared differences between the simulated spectra and the furthest 3σ bounded experimental curve as a function of the oxide's refractive index, using values for the layer thicknesses listed for $n = 1.610$ in Table I.

From Fig. 5 we deduce that the refractive index of the oxide is $n \sim 1.61$, but we are unable to accurately estimate its absorption coefficient. We note, however, that any narrow-band (linewidth between 20–500 cm^{-1}) absorption dips would be readily observed in the experiment if the associated absorption coefficient $(2\pi\kappa/\lambda)$ was greater than ~1000 cm^{-1}.

Table II lists values of the refractive index for oxidized $Al_xGa_{1-x}As$ reported in the associated references. For comparison, the refractive index of α–Al_2O_3 and gibbsite [γ–$Al(OH)_3$] are also listed. Our results are at the high range of those reported for other wet-oxidized AlGaAs layers. All of these results show that the refractive index of the converted semiconductor layers is significantly lower than that of crystalline α–Al_2O_3, and quite close to that of γ–$Al(OH)_3$. If hydrogen is a significant component in the wet-oxidized layers, the variations in the measured refractive indexes might be explained by small differences in the oxidation recipes used by different groups.

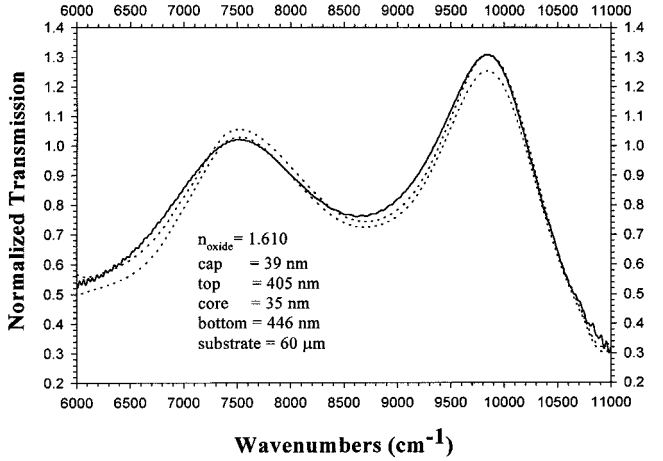

Fig. 4. Simulated versus experimental normalized transmission spectra for $n_{\text{oxide}} = 1.610$; the solid line corresponds to the simulation with the parameters listed above, and the dashed lines represent the uncertainty range (within $\pm 3\sigma$) of the average experimental transmission spectrum.

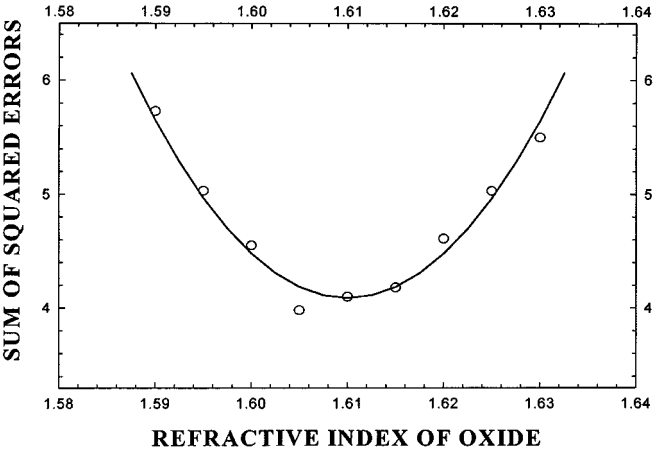

Fig. 5. Sum-of-squared deviations between simulated and experimentally bounded transmission spectra as a function of the simulated index of refraction of the oxide.

TABLE I
Comparison of Measured Thicknesses (SEM) with Those from the Simulations

n_{oxide}	cap layer thickness (nm)	top layer thickness (nm)	core layer thickness (nm)	bottom layer thickness (nm)
1.630	40	403	33	441
1.610	39	405	35	446
1.590	37	412	35	451
SEM	42±5	425±22	40±7	430±21

V. Conclusion

The optical constant of thick oxidized layers of $Al_{0.98}Ga_{0.02}As$ has been determined by fitting broad-band transmission spectra in the 900–1600 nm wavelength range. At a sensitivity of ~1000 cm^{-1}, the oxide exhibited no

TABLE II
LISTS OF REPORTED VALUES FOR THE INDEX OF REFRACTION OF OXIDIZED $Al_xGa_{1-x}As$. *THE STARTING MATERIAL FOR REFERENCE 16 IS ACTUALLY A DIGITAL ALLOY OF PERIOD 6 nm (5.5 nm AlAs, 0.5 nm $Al_{0.50}Ga_{0.50}As$)

Technique	Wavelengths (nm)	Starting Material	Refractive Index	Reference
ellipsometry	*not reported*	AlAs	1.5-1.6	11
ellipsometry	633	$Al_{0.80}Ga_{0.20}As$	1.63	12
ellipsometry	633	AlAs	1.56	13
ellipsometry	*not reported*	AlAs	1.50-1.56	14
ellipsometry	500-900	AlAs	1.50-1.54	15
ellipsometry	640-1640	$Al_{0.98}Ga_{0.02}As^*$	1.56-1.58	16
transmission	1000-1600	$Al_{0.98}Ga_{0.02}As$	1.59-1.63	*This work*
not reported	620-1771	α-Al_2O_3	1.742-1.767	21
not reported	*not reported*	γ-$Al(OH)_3$	1.587	22

narrow-band absorption, and its refractive index is 1.61 $\pm$ 0.02 over this range of wavelengths.

ACKNOWLEDGMENT

The M.Sc. work of P. Chen is acknowledged.

REFERENCES

[1] F. A. Kish, S. J. Caracci, N. Holonyak Jr., J. M. Dallesasse, K. C. Hsieh, and M. J. Ries, "Planar native-oxide index-guided $Al_xGa_{1-x}As$–GaAs quantum well heterostructure lasers," *Appl. Phys. Lett.*, vol. 59, pp. 1755–1757, Sept. 1991.

[2] D. L. Huffaker, C. C. Lin, J. Shin, and D. G. Deppe, "Resonant cavity light emitting diode with an Al_xO_y/GaAs reflector," *Appl. Phys. Lett.*, vol. 66, pp. 3096–3098, June 1995.

[3] Y. Hayashi, T. Mukaihara, N. Hatori, N. Ohnoki, A. Matsutani, F. Koyama, and K. Iga, "Record low-threshold index-guided InGaAs/AlGaAs vertical-cavity surface-emitting laser with a native oxide confinement structure," *Electron. Lett.*, vol. 31, pp. 560–562, Mar. 1995.

[4] P. D. Floyd, B. J. Thibeault, E. R. Hegblom, J. Ko, L. A. Coldren, and J. L. Merz, "Comparison of optical losses in dielectric-apertured vertical-cavity lasers," *IEEE Photon. Technol. Lett.*, vol. 8, pp. 590–592, May 1996.

[5] C. I. H. Ashby, J. P. Sullivan, K. D. Choquette, K. M. Geib, and H. Q. Hou, "Wet oxidation of AlGaAs: The role of hydrogen," *J. Appl. Phys.*, vol. 82, pp. 3134–3136, Sept. 1997.

[6] C. I. H. Ashby, J. P. Sullivan, P. P. Newcomer, N. A. Missert, H. Q. Hou, B. E. Hammons, M. J. Hafich, and A. G. Baca, "Wet oxidation of $Al_xGa_{1-x}As$: Temporal evolution of composition and microstructure and the implications for metal-insulator-semiconductor applications," *Appl. Phys. Lett.*, vol. 70, pp. 2443–2445, May 1997.

[7] S. Guha, F. Agachi, B. Pezeshki, J. A. Kash, D. W. Kisker, and N. A. Bojarczuk, "Microstructure of AlGaAs-oxide heterolayers formed by wet oxidation," *Appl. Phys. Lett.*, vol. 68, pp. 906–908, Feb. 1996.

[8] R. D. Twesten, D. M. Follstaedt, K. D. Choquette, and R. P. Schneider Jr., "Microstructure of laterally oxidized $Al_xGa_{1-x}As$ layers in vertical-cavity lasers," *Appl. Phys. Lett.*, vol. 69, pp. 19–21, July 1996.

[9] R. L. Naone and L. A. Coldren, "Surface energy model for the thickness dependence of the lateral oxidation of AlAs," *J. Appl. Phys.*, vol. 82, pp. 2277–2280, Sept. 1997.

[10] M. Ochiai, G. E. Giudice, H. Temkin, J. W. Scott, and T. M. Cockerill, "Kinetics of thermal oxidation of AlAs in water vapor," *Appl. Phys. Lett.*, vol. 68, pp. 1898–1900, Apr. 1996.

[11] F. A. Kish, S. J. Caracci, N. Holonyak Jr., J. M. Dallesasse, K. C. Hsieh, and M. J. Ries, "Planar native-oxide index-guided $Al_xGa_{1-x}As$–GaAs quantum well heterostructure lasers," *Appl. Phys. Lett.*, vol. 59, pp. 1755–1757, Sept. 1991.

[12] A. R. Sugg, E. I. Chen, N. Holonyak Jr., K. C. Hsieh, J. E. Baker, and N. Finnegan, "Effects of low-temperature anealing on the native oxide of $Al_xGa_{1-x}As$," *J. Appl. Phys.*, vol. 74, pp. 3880–3885, Sept. 1993.

[13] E. F. Schubert, M. Passlack, M. Hong, J. Mannerts, R. L. Opila, L. N. Pfeiffer, K. W. West, C. G. Bethea, and G. J. Zydzik, "Properties of Al_2O_3 optical coatings on GaAs produced by oxidation of epitaxial AlAs/GaAs films," *Appl. Phys. Lett.*, vol. 64, pp. 2976–2978, May 1994.

[14] M. H. MacDougal, H. Zhao, P. D. Dapkus, M. Ziari, and W. H. Steier, "Wide-bandwidth distributed Bragg reflectors using oxide/GaAs multilayers," *Electron. Lett.*, vol. 30, pp. 1147–1149, July 1997.

[15] P. Heremans, M. Kuijk, R. Windisch, J. Vanderhaegen, H. De Neve, R. Vounckx, and G. Borghs, "Angular spectroscopic analysis: An optical characterization technique for laterally oxidized AlGaAs layers," *J. Appl. Phys.*, vol. 82, pp. 5265–5267, Nov. 1997.

[16] K. J. Knopp, R. P. Mirin, D. H. Christensen, K. A. Bertness, A. Roshko, and R. A. Synowicki, "Optical constants of $(Al_{0.98}Ga_{0.02})_xAs_y$) native oxides," *Appl. Phys. Lett.*, vol. 73, pp. 3512–3514, Dec. 1998.

[17] M. Kanskar, P. Paddon, V. Pacradouni, R. Morin, A. Busch, J. F. Young, S. R. Johnson, J. MacKenzie, and T. Tiedje, "Two dimensional photonic lattice in an air-bridged semiconductor waveguide," *Appl. Phys. Lett.*, vol. 70, pp. 1438–1440, Aug. 1997.

[18] J. D. Joannopoulos, P. R. Villeneuve, and S. Fan, "Photonic crystals: Putting a new twist on light," *Nature*, vol. 386, pp. 143–149, Mar. 1997.

[19] P. W. Evans, J. J. Wierer, and N. Holonyak Jr., "$Al_xGa_{1-x}As$ native-oxide-based distributed Bragg reflectors for vertical cavity surface emitting lasers," *J. Appl. Phys.*, vol. 84, pp. 5436–5440, Nov. 1998.

[20] S. Adachi, "GaAs, AlAs, and $Al_xGa_{1-x}As$ material parameters for use in research and device applications," *J. Appl. Phys.*, vol. 58, pp. R1–R29, Aug. 1985.

[21] E. D. Palik, *Handbook of Optical Constants of Solids*. San Diego, CA: Academic, 1985, p. 770.

[22] L. D. Hart, *Alumina Chemicals Science and Technology Handbook*. OH: American Ceramic Society, 1990.

F. Sfigakis, photograph and biography not available at the time of publication.

P. Paddon, photograph and biography not available at the time of publication.

V. Pacradouni, photograph and biography not available at the time of publication.

M. Adamcyk, photograph and biography not available at the time of publication.

C. Nicoll, photograph and biography not available at the time of publication.

A. R. Cowan, photograph and biography not available at the time of publication.

T. Tiedje, photograph and biography not available at the time of publication.

Jeff F. Young, photograph and biography not available at the time of publication.